All-optical digital-to-analog converter based on cross-phase modulation with temporal integration

DEMING KONG[1,2], ZIHAN GENG[1,2], BENJAMIN FOO[1], VALERY ROZENTAL[1], BILL CORCORAN[1,2], AND ARTHUR JAMES LOWERY[1,2]

[1] Electro-Photonics Laboratory, Department of Electrical and Computer Systems Engineering, Monash University, VIC 3800, Australia
[2] Centre for Ultrahigh-bandwidth Devices for Optical Systems (CUDOS), Australia
[*] Corresponding authors: deming.kong@monash.edu

Compiled October 4, 2017

We propose and experimentally demonstrate an all-optical digital-to-analog converter (DAC) based on cross-phase modulation (XPM) with temporal integration. The scheme is robust to driving signal noise due to the low-pass filtering feature of the temporal integrator. The proof-of-concept experiment demonstrates the generation of pulse-amplitude modulation (PAM) sequences up to 8 levels. The performance of random PAM 2 and PAM 4 signals with different optical signal-to-noise ratios (OSNRs) of the binary driving signal is also investigated. The scheme is scalable for high-speed operation with appropriate dispersion profile of the nonlinear medium.

OCIS codes: *(060.2330) Fiber optics communications; (060.4080) Modulation; (060.4370) Nonlinear optics, fibers.*

http://dx.doi.org/10.1364/ol.XX.XXXXXX

The digital-to-analog converter (DAC) is a key component for generation of spectrally efficient multi-level modulation formats. Optical DACs have been proposed for their ability to achieve high baud rates and potentially low power consumption. Multi-modulator based schemes [1–6] offer flexibility in terms of number of bits, but are complex in terms of control mechanisms. Cross-phase modulation (XPM) based schemes, either using binary optical inputs with different amplitudes [7, 8], cascaded XPM stages [9], or different fiber lengths [10], have a weak tolerance to pump noise. Other schemes, based on summing of weighted multi-wavelength pulses [11], optical correlation [12], or micro-ring resonators [13, 14], are also potentially vulnerable to the noise of the driving sequences. Recently, we have proposed an electro-optical DAC, based on counter-propagating electrical binary pulses with optical pulses in a conventional optical Mach-Zehnder modulator (MZM) [15]. The optical pulses accumulate phase shifts according to the duration of the electrical pulses (i.e. temporal integration), suppressing noise and fluctuations from the electrical signal, resulting in improved signal quality.

In this paper, an all-optical DAC (AO-DAC), based on XPM with temporal integration, is proposed. Generation of PAM 2, 3, 4, 5, 6 & 8 sequences has been demonstrated at 1.25 GHz in a proof-of-concept experiment with 13-dBm pump power. The performance of random PAM 2 and PAM 4 signals has also been investigated with different pump optical signal-to-noise ratios (OSNRs), confirming noise suppression capability of the scheme. We also discuss paths to improving this scheme towards providing a high-fidelity and high-speed all-optical DAC.

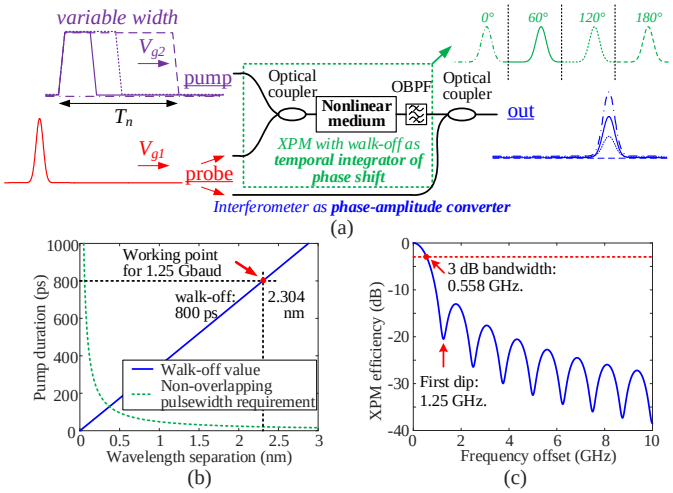

Fig. 1. (a) Principle of the proposed AO-DAC; (b) calculated walk-off and non-overlapping pulse-width requirement for 3.4 km DCF; (c) XPM efficiency at probe rate of 1.25 Gbaud.

Fig. 1 (a) illustrates the principle of the proposed AO-DAC with two main components, including an XPM-based temporal integrator and an interferometer-based phase-to-amplitude converter. For the XPM-based temporal integrator, a probe pulse sequence and a coded pump signal are coupled in a nonlinear medium. The probe is then phase-modulated by the pump due to XPM. The key idea of this scheme is to introduce an appropriate walk-off between the probe and the pump so that the probe experiences the pump-pulse-induced phase rotation from the leading edge to the falling edge of the pump (or vice versa). In this way, the probe is modulated not by the amplitude of the pump but rather by the integration of the optical power across the designed walk-off time. The integrated phase modulation

from the pump pulse can then be expressed as:

$$\phi_n = 2\gamma\sqrt{\eta_{XPM}}L_{eff}\frac{\int_0^{T_w} P(t)dt}{T_w}, \quad (1)$$

where γ is the nonlinear coefficient of the medium; η_{XPM} is the XPM efficiency [16]; L_{eff} is the effective length of the nonlinear medium given by $L_{eff} = (1 - e^{\alpha L})/\alpha$; $P(t)$ is the optical power profile of the pump pulse; T_w is the walk-off time. Considering T_n is the actual pump pulse-width within T_w and $T_n \leqslant T_w$, the integral will differ for various T_w durations if either the optical power profile, $P(t)$, or the pulse-width, T_n, is adjusted. For example, if the pump is a multi-level signal with a fixed duration $T_n = T_p$, the probe would be phase-modulated depending on the input level of the pump $P_n(t), (n = 1, 2, ...N)$. Alternatively, if the pump is a binary non-return-to-zero (NRZ) signal and N symbols with a variable total duration $T_n \leqslant T_w, (n = 1, 2, ...N)$ are treated as one input digital word, the probe will walk off with each digital word and the accumulated phase will differ according to T_n. In other words, the pump pulse-width could be adjusted in discrete steps, by binary NRZ modulation, to get different modulation depths. To get a maximum modulation efficiency, the maximum pulse-width of the pump should equal to T_w. The probe should be aligned with either leading or falling edge of the pump if it travels slower or faster than the pump, respectively. Followed the temporal integrator, an interferometer is used for phase-amplitude conversion, generating analog output levels according to the phase modulation depth [15].

Fig. 1 (b) gives an example of the calculated walk-off values from a 3.4-km dispersion compensating fiber (DCF) when the pump wavelength is fixed around 1550 nm ($\alpha = 0.765$ dB/km, D $= -107.4$ ps/nm/km, S $= -0.3567$ ps/nm^2/km, @1566 nm). The dashed curve gives the minimum NRZ pulse-width for the pump and the probe without overlapping in the frequency domain. To easily filter out the probe after phase modulation, a wavelength separation of 2.304 nm is chosen, resulting in a walk-off value of $T_w = 800$ ps. Then the repetition rate of the probe is $1/800$ ps $= 1.25$ GHz.

Fig. 1 (c) illustrates the calculated efficiency of the XPM effect [16] against frequency offset from the center of the pump. Firstly, this figure indicates that the temporal integrator can be represented by a rectangular window of width T_w, which will suppress most of the out-of-band noise from the pump. Secondly, as the temporal integrator acts as a low-pass filter, the operating baud rate of the DAC is limited, such that the phase modulation from the transitions of the pump will be filtered and distorted. However, as long as the probe experiences the same number of rising and falling transitions of the pump during the walk-off time T_w, the amount of nonlinear phase modulation will be exactly the same and will not effect the phase-to-amplitude conversion for each generated level. This requires special coding for the pump signal. Two complementary pumps can also be used to cancel out the effect of transitions. If four output levels are required, the combined duration of four symbols of the input binary waveform can be treated as one pump symbol. With the coding scheme shown in Tab. 1, the probe will experience only one rising edge and one falling edge for each T_w. Note that an extra guard interval is inserted to accommodate the probe pulse.

Fig. 2 (a) shows the proof-of-concept experimental setup, consisting of five functional modules: pump generation, probe generation, noise loading, all-optical DAC, and baseband receiver. For the implementation of the AO-DAC, a nonlinear optical loop mirror (NOLM) is used. Since dispersion in optical fibers is

Table 1. Example coding scheme of the pump for 4 levels DAC.

Digital word T_w	Phase modulation	Analog output level
0, 0, 0, 0	ϕ_0	3
1, 0, 0, 0	ϕ_1	2
1, 1, 0, 0	ϕ_2	1
1, 1, 1, 0	ϕ_3	0

isotropic, the clockwise propagated probe pulses, modulated by the pump signal experience the same amount of dispersion as the counterclockwise propagated probe pulses, so that the pulse shape of the output can be preserved. However, the counterclockwise propagated probe pulses are also modulated by the pump signal. But, since the walk-off for counter-propagation is so large, the counterclockwise propagated probe pulses will experience the pump signal as a continuous wave and will have a constant phase rotation θ if the pump average power is constant. As illustrated in Fig. 2 (b), the filtered output of the NOLM is a vector sum of both clockwise and counterclockwise modulated pulses, this counter-propagating phase rotation will result in unwanted level shifts or even level jumps at the output of the NOLM, affecting the level distribution of the AO-DAC generated signal. The counter-propagation-induced level shifts can be solved by carefully adjusting the polarization controller in the NOLM (PC 3) and the polarization controller for the probe (PC 2) to intentionally introduce some residual output. Counter-propagation-induced level jumps can be eliminated by precoding of the pump. These issues related to counter-propagating only exist in a NOLM-based setup. In the experiment, a 3.4-km DCF with the same parameters described previously is inserted as the nonlinear medium. The measured static extinction ratio of the NOLM without the pump was 32 dB.

For the generation of the probe, an ECL running at 1552.539 nm is externally modulated to produce 100 ps pulses, at a repetition rate of 1.25 GHz, before it is amplified, filtered, and aligned with the guard interval of the pump. PC 2 is used to adjust the initial polarization state of the probe to the NOLM. For the generation of the pump signal, another ECL working at 1550.235 nm, with a wavelength separation of 2.304 nm from the probe, is used to get a total walk-off of 800 ps in the DCF. The ECL is modulated by a coded pump sequence with a guard interval of 200 ps between adjacent symbols. The noise loading module composed of an EDFA, a 100-GHz rectangular-shaped filter implemented with a WSS, a booster EDFA, and a VOA, is used to load an appropriate amount of noise power to the pump signal for performance investigation. The in-band OSNR of the pump is calculated using the "Signal On/Off" method [17]. The polarization of the noise-loaded pump signal is adjusted by PC 1 before it is amplified and filtered by cascaded high-pass and 1-nm band-pass optical filters with a bandwidth of ~ 100 GHz. A VOA is inserted before the NOLM to adjust the power of the pump signal. The baseband receiver includes an EDFA, a 100-GHz OBPF, a 70-GHz PD, and a real-time oscilloscope set to 10-GHz electrical bandwidth with 40-GSa/s sampling rate. The EDFA used for the receiver has a noise figure of 5.5 dB, and is set to give a controlled output power of 3 dBm.

Fig. 2 (c) shows the optical spectra at the output of the NOLM. The power difference between NOLM "on" (with 13-dBm pump power) and "off" states (no pump) from the spectra is 15 dB. Considering the optical spectra correspond to average power, the dynamic extinction ratio is expected to be around 18 dB, indicating that the modulation depth is limited. If the pump power keeps increasing, severe stimulated Brillouin scattering (SBS)

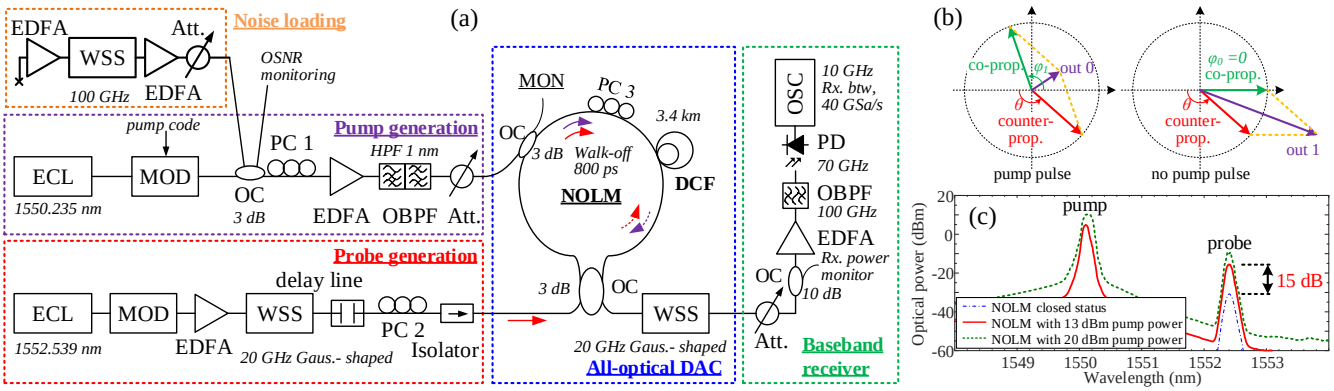

Fig. 2. (a) Experimental setup (ECL: external cavity laser; MOD: modulator; OC: optical coupler; VOA: variable optical attenuator; WSS: wavelength-selective switch; PC: polarization controller; OBPF: optical bandpass filter; PD: photo-detector; OSC: oscilloscope); (b) Illustration on the effect of counter-propagation in NOLM; (c) Optical spectra of the pump and the probe.

effects can be observed, resulting in random phase modulation of the probe, degrading the signal quality. In this experimental setup, the SBS threshold was found to be around 15 dBm.

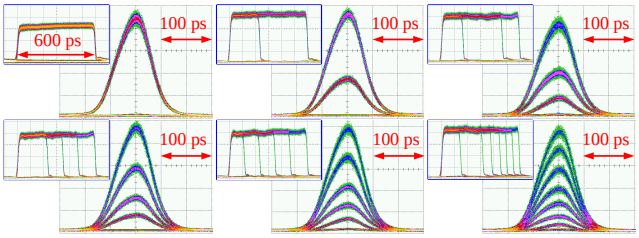

Fig. 3. Eye diagrams of the AO-DAC generated PAM 2, 3, 4, 5, 6, & 8 sequences. Insets show the corresponding eye diagrams of the pumps.

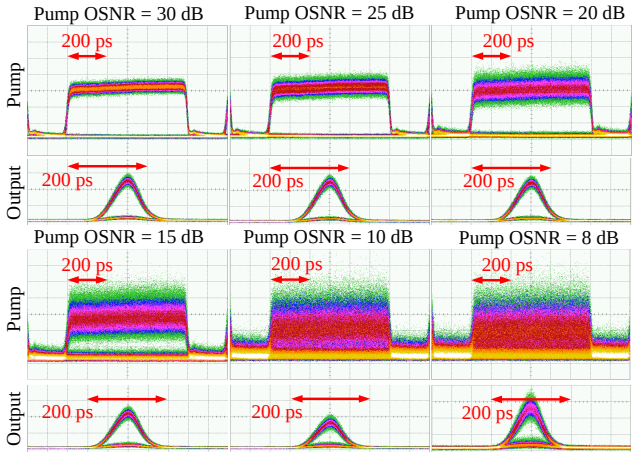

Fig. 4. Eye diagrams of the pump and the AO-DAC generated PAM 2 (OOK) signal with different pump OSNR values.

Fig. 3 shows the eye diagrams of the PAM 2, 3, 4, 5, 6, & 8 sequences generated with repeated binary pump sequences, demonstrating the scalability of the scheme. The insets show corresponding eye diagrams of the pump sequences. Owing to the phase rotation, introduced by counter-propagating and nonlinear transfer function of phase-to-amplitude conversion, the pump width has been adjusted to obtain a more evenly spaced output levels. In addition, these PAM sequences were all achieved with an average pump power of 13 dBm, indicating that the output of directly modulated lasers could in principle be used for the pump without requiring amplification.

Fig. 4 illustrates eye diagrams of the pump and the AO-DAC generated PAM 2 (OOK) signals under different pump OSNR values, with random binary pump data with 5456 words. Note that the calculated OSNR using the "Signal On/Off" method measures the in-band noise only. Since the optical filters used for the pump signals are off-the-shelf thin-film filters, there is a significant amount of out-of-band noise added to the pump. However, the temporal integrator based AO-DAC strongly attenuates the out-of-band noise. As can be observed from the eye diagrams, all the output signals show significantly improved eye opening.

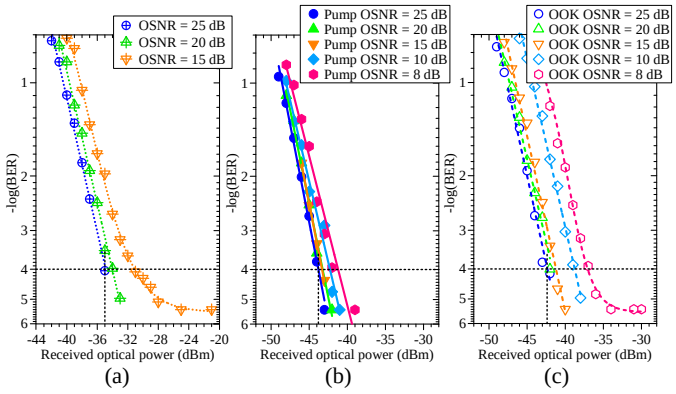

Fig. 5. BER of (a) the pump signals, (b) the AO-DAC generated PAM 2 (OOK) signals, and the (c) directly modulated RZ-OOK signals, with different OSNR values.

Fig. 5 (a) and (b) demonstrate the BER performance of the pump signals and the AO-DAC generated PAM 2 signals for different pump OSNRs. The performance of the AO-DAC generated PAM 2 signal under a pump OSNR of 25 dB is 9-dB better due to the elimination of the out-of-band noise and NRZ-to-return-to-zero (RZ) conversion. Fig. 5 (c) shows the BER performance of the directly modulated RZ-OOK signal with exactly the same shape with the AO-DAC generated PAM 2 signal for comparison. The PAM 2 signal from the AO-DAC outperforms the directly modulated RZ-OOK signal by at least 1.5 dB at a BER value of 10^{-4}, under various OSNR values. This confirms the noise suppression capability by temporal integration.

Fig. 6 depicts eye diagrams of the pump and the AO-DAC generated PAM 4 signals with different pump OSNR values using random binary pump data with 5456 words. As with the PAM 2 signal, the out-of-band noise is heavily suppressed.

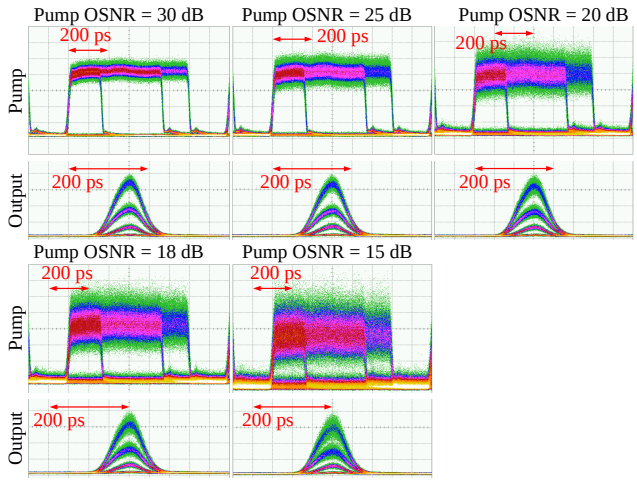

Fig. 6. Eye diagrams of the pump and the AO-DAC generated PAM 4 signal with different pump OSNR values.

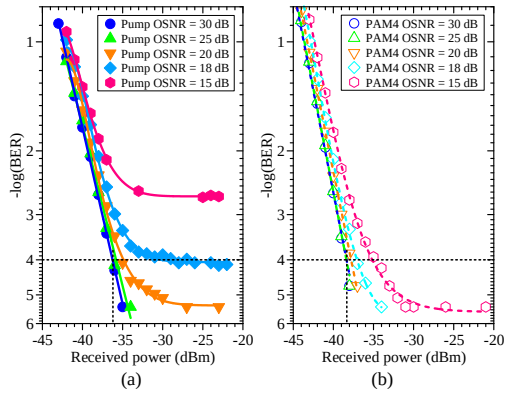

Fig. 7. BER of (a) the AO-DAC generated PAM 4 signals, and the (b) directly modulated RZ-PAM 4 signals, with different OSNR values.

Fig. 7 (a) shows the BER performance of the AO-DAC generated PAM 4 signals with different pump OSNR values. Fig. 7 (b) shows the BER performance of directly modulated RZ-PAM 4 signals (fully modulated with optimized level shifting) for different OSNR values. The AO-DAC generated PAM 4 signal performs approximately 2-dB worse with 30 dB OSNR at a BER value of 10^{-4}. We attribute the lower performance of the AO-DAC generated PAM 4 signal to the nonlinear transfer function intrinsic to the NOLM, as well as the limited extinction ratio.

There are a number of improvements that can be made to the proposed scheme to improve the AO-DAC performance. The extinction ratio of the NOLM is partly limited by the SBS, effectively providing an upper limit to pump power. This is further complicated by the counter-propagation-induced phase shift in the NOLM. Both the counter-propagating phase shift, and the limited bandwidth of the AWG used to modulate the pump, make it difficult to perform a perfect level shifting to compensate for the intrinsic nonlinear transfer function of the NOLM, resulting in degraded performance when targeting multilevel output signals. To improve the extinction ratio of the output, switching to a high-SBS-threshold nonlinear material would help to induce full switching, and using an interferometer-based setup shown in Fig. 1 instead of a NOLM would remove the effect of the counter-propagation phase shift.

All-optical DACs often target high bandwidth applications. The AO-DAC scheme we propose here is not intrinsically limited in bandwidth, and can be easily adapted to higher baud rates by simply changing the nonlinear material with reduced dispersion and applying high-speed NRZ-shaped signal [18] for the pump. If a 1-km highly nonlinear fiber with a dispersion profile of $D = -0.5$ ps/nm/km, $S = 0.016$ ps/nm^2/km (@1550 nm) is utilized, 50 Gbaud operation can be realized with a walk-off value of 20 ps and a wavelength separation of 40 nm (pump@1530 nm). Moreover, we note that the coding scheme shown in Table 1 results in a reduced spectral efficiency. As the output signal is a low duty-cycle RZ signal, this loss in spectral efficiency can be regained by time-division multiplexing the output signal.

In conclusion, AO-DAC based on XPM with temporal integration has been proposed and demonstrated through a proof-of-concept experiment. Generation of PAM 2, 3, 4, 5, 6 & 8 sequences has been experimentally demonstrated at 1.25 GHz with a NOLM setup. The performance of PAM 2 and PAM 4 signals has also been investigated using random pump data for different OSNR values, proving the noise suppression capability. While the AO-DAC proposed here shows significant resilience to noise drive signals, we believe that there are further applications for walk-off induced temporal integrator, such as OSNR monitoring, and generation of advanced modulation formats.

Funding. The Australian Research Council's CUDOS – ARC Centre of Excellence for Ultrahigh bandwidth Devices for Optical Systems (CE110001018); ARC Laureate Fellowship (FL130100041).

REFERENCES

1. T. Saida, K. Okamoto, H. Yamada, K. Takiguchi, T. Shibata, A. Sugta, and K. Uchiyama, in *Optical Fiber Communication Conference (OFC)* (Optical Society of America, 2001), paper WY2–1.
2. A. Leven, L. Jie, J. Lee, T. Kun-Yii, Y. Baeyens, and Y. K. Chen, in *The 17th Annual Meeting of the IEEE Lasers and Electro-Optics Society (LEOS), 2004*, paper TuN2.
3. P. K. Kondratko, A. Leven, C. Young-Kai, L. Jie, K. Ut-Va, T. Kun-Yii, and L. Jaesik, IEEE Photonics Technology Letters **17**, 2727 (2005).
4. X. Yu, K. Wang, X. Zheng, and H. Zhang, Electronics Letters **43**, 1044 (2007).
5. T. Sakamoto and A. Chiba, IEEE Journal of Selected Topics in Quantum Electronics **16**, 1140 (2010).
6. J. Liao, H. Wen, X. Zheng, P. Xiang, H. Zhang, and B. Zhou, IEEE Photonics Technology Letters **25**, 126 (2013).
7. A. Maruta and N. Hashimoto, in *Optical Fiber Communication Conference (OFC)* (Optical Society of America, 2012), paper OM3B.1.
8. G. Huang, Y. Miyoshi, A. Maruta, Y. Yoshida, and K.-I. Kitayama, Journal of Lightwave Technology **30**, 1342 (2012).
9. S. Oda and A. Maruta, IEEE Photonics Technology Letters **18**, 703 (2006).
10. J. M. Jeong and M. E. Marhic, Optics Communications **91**, 115 (1992).
11. Y. Peng, H. Zhang, Y. Zhang, and M. Yao, IEEE Photonics Technology Letters **20**, 2135 (2008).
12. T. Nishitani, T. Konishi, H. Furukawa, and K. Itoh, Optics Express **13**, 10310 (2005).
13. L. Yang, J. Ding, Q. Chen, P. Zhou, F. Zhang, and L. Zhang, Optics Letters **39**, 5736 (2014).
14. R. Li, D. Patel, A. Samani, E. El-Fiky, Z. Xing, M. Morsy-Osman, and D. V. Plant, IEEE Photonics Technology Letters **29**, 1046 (2017).
15. A. J. Lowery, Optics Express **22**, 26429 (2014).
16. T. K. Chiang, N. Kagi, M. E. Marhic, and L. G. Kazovsky, Journal of Lightwave Technology **14**, 249 (1996).
17. D. Gariépy, S. Searcy, G. He, and S. Tibuleac, Optics Express **24**, 20156 (2016).
18. H. Hu, P. Münster, E. Palushani, M. Galili, K. Dalgaard, H.C. Mulvad, P. Jeppesen, and L. Oxenløwe, in *Optical Fiber Communication Conference (OFC)* (Optical Society of America, 2012), paper PDP5C.7.

FULL REFERENCES

1. T. Saida, K. Okamoto, H. Yamada, K. Takiguchi, T. Shibata, A. Sugta, and K. Uchiyama, "Optical pulse pattern recognition circuit based on an optical digital-to-analog converter on a planar lightwave circuit," in *Optical Fiber Communication Conference (OFC)* (Optical Society of America, 2001), paper WY2–1.
2. A. Leven, L. Jie, J. Lee, T. Kun-Yii, Y. Baeyens, and Y. K. Chen, "A 12.5 Gsample/s optical digital-to-analog converter with 3.8 effective bits," in *The 17th Annual Meeting of the IEEE Lasers and Electro-Optics Society (LEOS), 2004*, paper TuN2.
3. P. K. Kondratko, A. Leven, C. Young-Kai, L. Jie, K. Ut-Va, T. Kun-Yii, and L. Jaesik, "12.5 GHz optically sampled interference-based photonic arbitrary waveform generator," IEEE Photonics Technology Letters **17**, 2727–2729 (2005).
4. X. Yu, K. Wang, X. Zheng, and H. Zhang, "Incoherent photonic digital-to-analogue converter based on broadband optical source," Electronics Letters **43**, 1044–1045 (2007).
5. T. Sakamoto and A. Chiba, "Coherent synthesis of optical multilevel signals by electrooptic digital-to-analog conversion using multiparallel modulator," IEEE Journal of Selected Topics in Quantum Electronics **16**, 1140–1149 (2010).
6. J. Liao, H. Wen, X. Zheng, P. Xiang, H. Zhang, and B. Zhou, "Novel bipolar photonic digital-to-analog conversion employing differential phase shift keying modulation and balanced detection," IEEE Photonics Technology Letters **25**, 126–128 (2013).
7. A. Maruta and N. Hashimoto, "Experimental demonstration of all-optical modulation format conversion from NRZ-OOK to RZ-8APSK based on fiber nonlinearity," in *Optical Fiber Communication Conference (OFC)* (Optical Society of America, 2012), paper OM3B.1.
8. G. Huang, Y. Miyoshi, A. Maruta, Y. Yoshida, and K.-I. Kitayama, "All-optical OOK to 16-QAM modulation format conversion employing nonlinear optical loop mirror," Journal of Lightwave Technology **30**, 1342–1350 (2012).
9. S. Oda and A. Maruta, "All-optical digital-to-analog conversion using nonlinear optical loop mirrors," IEEE Photonics Technology Letters **18**, 703–705 (2006).
10. J. M. Jeong and M. E. Marhic, "All-optical analog-to-digital and digital-to-analog conversion implemented by a nonlinear fiber interferometer," Optics Communications **91**, 115–122 (1992).
11. Y. Peng, H. Zhang, Y. Zhang, and M. Yao, "Photonic digital-to-analog converter based on summing of serial weighted multiwavelength pulses," IEEE Photonics Technology Letters **20**, 2135–2137 (2008).
12. T. Nishitani, T. Konishi, H. Furukawa, and K. Itoh, "All-optical digital-to-analog conversion using pulse pattern recognition based on optical correlation processing," Optics Express **13**, 10310–10315 (2005).
13. L. Yang, J. Ding, Q. Chen, P. Zhou, F. Zhang, and L. Zhang, "Demonstration of a 3-bit optical digital-to-analog converter based on silicon microring resonators," Optics Letters **39**, 5736–5739 (2014).
14. R. Li, D. Patel, A. Samani, E. El-Fiky, Z. Xing, M. Morsy-Osman, and D. V. Plant, "Silicon photonic ring-assisted MZI for 50 Gb/s DAC-less and DSP-free PAM-4 transmission," IEEE Photonics Technology Letters **29**, 1046–1049 (2017).
15. A. J. Lowery, "All-optical DAC using counter-propagating optical and electrical pulses in a Mach-Zehnder modulator," Optics Express **22**, 26429–26437 (2014).
16. T. K. Chiang, N. Kagi, M. E. Marhic, and L. G. Kazovsky, "Cross-phase modulation in fiber links with multiple optical amplifiers and dispersion compensators," Journal of Lightwave Technology **14**, 249–260 (1996).
17. D. Gariépy, S. Searcy, G. He, and S. Tibuleac, "Non-intrusive OSNR measurement of polarization-multiplexed signals with spectral shaping and subject to fiber non-linearity with minimum channel spacing of 37.5GHz," Optics Express **24**, 20156–20166 (2016).
18. H. Hu, P. Münster, E. Palushani, M. Galili, K. Dalgaard, H.C. Mulvad, P. Jeppesen, and L. Oxenløwe, "640 Gbaud NRZ-OOK data signal generation and 1.19 Tbit/s PDM-NRZ-OOK field trial transmission," in *Optical Fiber Communication Conference (OFC)* (Optical Society of America, 2012), paper PDP5C.7.